Thermodynamic Interrogation of a Folding Disease. Mutant Mapping of Position 107 in Human Carbonic Anhydrase II Linked to Marble Brain Disease

Karin Almstedt, Lars-Göran Mårtensson, Uno Carlsson, and Per Hammarström*

IFM-Department of Chemistry, Linköping University, 581 83 Linköping, Sweden

Received August 23, 2007; Revised Manuscript Received November 22, 2007

ABSTRACT: Marble brain disease (MBD) also known as Guibaud−Vainsel syndrome is caused by autosomal recessive mutations in the human carbonic anhydrase II (HCA II) gene. HCA II is a 259 amino acid single domain enzyme and is dominated by a 10-stranded β-sheet. One mutation associated with MBD entails the H107Y substitution where H107 is a highly conserved residue in the carbonic anhydrase protein family. We have previously demonstrated that the H107Y mutation is a remarkably destabilizing folding mutation [Almstedt et al. (2004) *J. Mol. Biol. 342*, 619−633]. Here, the exceptional destabilization by the H107Y mutation has been further investigated. A mutational survey of position H107 and a neighboring conserved position E117 has been performed entailing the mutants H107A, H107F, H107N, E117A and the double mutants H107A/E117A and H107N/E117A. All mutants were severely destabilized versus GuHCl and heat denaturation. Thermal denaturation and GuHCl phase diagram and ANS analyses showed that the mutants shifted HCA II toward populating ensembles of intermediates of molten globule type under physiological conditions. The native state stability of the mutants was in the following order: wt > H107N > E117A > H107A > H107F > H107Y > H107N/E117A > H107A/E117A. In conclusion: (i) H107N is least destabilizing likely due to compensatory H-bonding ability of the introduced Asn residue. (ii) Double mutant cycles surprisingly reveal additive destabilization of H107N and E117A showing that H107 and E117 are independently stabilizing the folded protein. (iii) H107Y and H107F are exceptionally destabilizing due to bulkiness of the side chains whereas H107A is more accommodating, indicating long-range destabilizing effects of the natural pathogenic H107Y mutation.

There are hundreds of loss-of-function diseases that are caused by protein misfolding. These include well-known diseases such as p53 tumor suppressor related cancer, cystic fibrosis, and phenylketonuria, all caused by somatic or familial mutations. The molecular rationale of the majority of loss-of-function folding diseases are hampered by the lack of specific protein folding/misfolding information of the proteins involved. Human carbonic anhydrase II (HCA II[1]) has been a model protein for protein folding studies for a long time, and its pathways for folding, misfolding, aggregation, and interactions with molecular chaperones have been mapped by us (*1*−*12*).

One orphan loss-of-function folding disease is carbonic anhydrase II deficiency syndrome (CADS), also known as marble brain disease (MBD) or Guibaud−Vainsel syndrome. This disease is due to the misfolding of human carbonic anhydrase II, and it gives rise to osteopetrosis in combination with renal tubular acidosis (RTA), cerebral calcification, growth retardation, dental malocclusion, and in most of the cases also mental retardation (*13*). Twenty three different mutations in the HCA II gene have been reported to cause CADS (*14*−*16*). One of the mutations first described in a Belgian patient homozygous for a C to T substitution in exon 3 resulted in the replacement of a highly conserved His at position 107 by Tyr (*17*). This mutation has since been reported in three more families from Italy and Japan where the patients show a range in disease severity including mental disturbance. All patients had RTA and osteopetrosis.

The H107Y mutation has been carefully characterized by us (*18*), and it was shown by activity measurements, inhibitor binding, intrinsic Trp fluorescence, and NMR measurements that this mutant is folded at low temperature (4 °C), but that the mutant structure is more dynamic than the wild type enzyme. The native state stability of the mutant was decreased by 9.2 kcal/mol and the midpoint of denaturation (T_m) had decreased by a staggering 39 °C. To our knowledge this is the greatest degree of protein destabilization measured for a natural occurring human mutation. It was also shown that this mutant folds via a new intermediate, that we called molten globule light. The molten globule light intermediate is more folded than the classical molten globule characterized for HCA II and hence exposes less hydrophobic surface area. This intermediate is not aggregation prone at low protein concentrations but is very prone to aggregate at high protein concentrations. We also showed that the folding equilibrium can be shifted toward the native state by binding of the small-molecule drug acetazolamide.

* Corresponding author. Phone (46)-13-285690, fax (46)-13-281399, e-mail: perha@ifm.liu.se (P. Hammarström).

[1] Abbreviations: ANS, 8-anilino-1-naphthalenesulfonic acid; CADS, carbonic anhydrase II deficiency syndrome; HCA II, human carbonic anhydrase II; HCA II_{pwt}, human carbonic anhydrase II pseudo wild type entailing a C206S mutation; MBD, marble brain disease; NGCA, carbonic anhydrase from *Nesseria gonorrhoea*; near-UV CD, circular dichroism in the wavelength region 240-320 nm; RTA, renal tubular acidosis.

10.1021/bi701720p CCC: $40.75 © 2008 American Chemical Society
Published on Web 01/12/2008

To further investigate the devastating effect of the H107Y mutation, a mutational study of this position and a neighboring interacting position E117 was performed in this work. Double mutants and small molecule binding interactions were employed to elucidate the thermodynamic stability contribution of the H107 residue. The enormously destabilizing effects of the H107Y mutation is not due to loss of specific interactions with residue E117; instead it is caused by long-range sterical destabilizing effects of the bulky tyrosine residue.

MATERIALS AND METHODS

Materials. Ultra Pure GuHCl was obtained from ICN Biomedicals and the concentration of all GuHCl solutions was determined by refractometrical measurements (*19*). 8-Anilino-1-naphthalenesulfonic acid (ANS) was obtained from Sigma, and isopropyl β-D-thiolgalactopyranoside (IPTG) was obtained from Saveen.

Production and Purification of Mutants. Site-directed mutagenesis was performed with the Quik-Change site-directed mutagenesis kit from Stratagene. Oligonucleotide primers were ordered from DNA Technology A/S and TAG Copenhagen A/S. The mutageneses were performed with pseudo wild type HCA II (HCA II_{pwt}) as a template containing the mutation C206S, possessing the same properties as the wild type HCA II. The following primers were used to generate the mutants:

H107F

5′ GAT GGA CAA GGT TCA GAG **TTT** ACT GTG GAT AAA AAG AAA TAT GC 3′

5′ GCA TAT TTC TTT TTA TCC ACA GT**A AA**C TCT GAA CCT TGT CCA TC 3′

H107A

5′ GAT GGA CAA GGT TCA GAG **GCT** ACT GTG GAT AAA AAG AAA TAT GC 3′

5′ GCA TAT TTC TTT TTA TCC ACA GT**A GC**C TCT GAA CCT TGT CCA TC 3′

H107N

5′ GAT GGA CAA GGT TCA GAG **AAT** ACT GTG GAT AAA AAG AAA TAT GC 3′

5′ GCA TAT TTC TTT TTA TCC ACA GT**A TT**C TCT GAA CCT TGT CCA TC 3′

E117A

5′ GTG GAT AAA AAG AAA TAT GCT GCA **GCA** CTT CAC TTG GTT CAC TGG 3′

5′ CCA GTG AAC CAA GTG AAG **TGC** TGC AGC ATA TTT CTT TTT ATC CAC 3′

E. coli BL21/DE3 containing the mutated plasmid pACA was grown in 2× Luria Broth medium with 60 μg/mL ampicillin at 37 °C, until $A_{660\ nm}$ was 0.8, and then placed at room temperature (22 °C). When the medium had cooled, the protein production was induced by adding IPTG and $ZnSO_4$ to a final concentration of 0.5 mM each, and the protein production was stopped after 4 h. The cells were lysed by a freeze−thaw method using an X-Press of type X-25 from BioX, and the supernatant was run on an affinity chromatography column at 4 °C to purify the mutant protein (*20*). The protein concentration was determined by measurement of A_{280}, using $\epsilon_{280} = 54\,800\ M^{-1}\ cm^{-1}$.

Activity Measurements. The activity of the mutants and HCA II_{pwt} was measured by the colorimetric CO_2-hydration method described by Rickli et al. (*21*).

Stability Measurements. To determine the stability of the mutants toward thermal denaturation, the intrinsic Trp fluorescence was measured in a 1 cm path-length quartz cuvette, by a Hitachi F-4500 fluorescence spectrophotometer using a thermostated cell. The excitation wavelength was 295 nm, and the spectra were collected between 305 and 450 nm with both the entrance and exit slits set to 5 nm. The protein concentration was 0.8 μM in 100 mM Na-borate buffer, pH 7.5. The measurements started at 4 °C, and the temperature was increased by 5 °C and held for 7 min to allow equilibration before the next measurement. The thermal stability was also determined by activity measurements, using the CO_2-hydration assay above.

To determine the stability of the mutants toward denaturation by GuHCl, the enzymes (0.8 μM, 100 mM Tris-H_2SO_4 and pH 7.5) were incubated for 20 h at 4 °C in various concentrations of GuHCl. Thereafter Trp fluorescence spectra were collected at 4 °C, using the same instrument parameters as above. The data were fitted to two separate unfolding transitions for calculation of the Gibbs free energy of unfolding for the transitions from the native, N, to the intermediate, I, and from the I to the unfolded, U, state, respectively (ΔG_{NI} and ΔG_{IU}). A linear dependence of the GuHCl concentration of the Gibbs free energy of unfolding was assumed for both transitions (*22*) according to the formulas:

$$\Delta G_{NI} = \Delta G_{NI}^{H_2O} - m_{NI}[\mathrm{GuHCl}] \quad (1)$$

$$\Delta G_{IU} = \Delta G_{IU}^{H_2O} - m_{IU}[\mathrm{GuHCl}] \quad (2)$$

where ΔG^{H_2O} denotes the Gibbs free energy of unfolding of the mutant in the absence of denaturant and m denotes the slope of the dependence of the stability on the denaturant concentration which reflects the cooperativity of folding and is proportional to the exposure of solvent accessible surface area (*23*).

The stability of the mutants toward denaturation by GuHCl was also measured as above when the mutants were incubated for 10 min with the inhibitor acetazolamide (final concentration 10 μM) before denaturation by GuHCl. The denaturation data in the presence and absence of inhibitor were used for calculation of the stability of the native conformation using formula 1. The stabilizing effect of acetazolamide binding only affects the first transition, due to selective binding to the native state, and was calculated from the formula:

$$\Delta\Delta G^{Ac} = \Delta G_{NI}^{Ac} - \Delta G_{NI} \quad (3)$$

where $\Delta\Delta G^{Ac}$ denotes the stabilizing energy of acetazolamide and ΔG_{NI}^{Ac} denotes the Gibbs free energy of unfolding of the mutant in the presence of 10 μM acetazolamide.

Phase diagrams were obtained by plotting the Trp-fluorescence intensities for different GuHCl concentrations at 320 nm (I 320) versus the intensity at 365 nm (I 365). Linear shifts in either parameter versus GuHCl are correlated to conformational transitions as described by the Uversky group (*24*).

ANS Measurements. 8-Anilino-1-naphthalenesulfonic acid, ANS, was added to a final concentration of 40 μM just prior to the measurements, in a 1 cm path-length quartz cuvette, to samples containing the mutant proteins (0.8 μM, 100 mM Tris-H_2SO_4 and pH 7.5) with or without preincubation with acetazolamide (final concentration 10 μM) in various concentration of GuHCl. The excitation wavelength was 360 nm and the emission spectra were recorded in the wavelength region 380−600 nm, with both entrance and exit slits set to 10 nm. The area of the ANS fluorescence intensities were determined in the wavelength region 460−510 nm and were plotted versus the GuHCl concentration. The integrated area of the ANS fluorescence intensity in the range of molten globule formation (0−2 M GuHCl) was determined for each mutant.

Aggregation Measurements. Light scattering was used to determine the formation of large aggregates. The protein sample (1.7 μM, 100 mM Tris-H_2SO_4 and pH 7.5) was illuminated by light of 330 nm, and the intensity of the reflected light (332 nm) was measured at right angle from the incoming light, in a 1 cm path-length quartz cuvette. The temperature was increased and controlled as described above. The entrance slit was set to 10 nm, and the exit slit was set to 1 nm.

RESULTS

Selection of Mutants. The positions of H107 and E117 are in the vicinity of the active site with a distance of 7.6 Å and 10.2 Å to the zinc atom. Among α-carbonic anhydrases the positions of H107 and E117 are totally invariant in higher organisms. The only exceptions that we have found are in bacterial carbonic anhydrases. Here variations are found in carbonic anhydrase from *Neisseria gonorrheae* (NGCA) and carbonic anhydrase from *Helicobacter pylori* (25).

Five single mutants (H107A, H107N, H107F, H107Y, and E117A) and two double mutants (H107N/E117A and H107A/E117A) were generated using the pseudo-wild type HCA II_{pwt} as a background. The HCA II_{pwt} entails a C206S mutation that renders HCA II cysteine free and shows indistinguishable folding and functional properties from the wild type protein (*4*, *5*, *7*−*10*). The mutant H107A was selected to remove side chain interactions, such as the formation of hydrogen bonds and to minimize sterical disturbance. H107F was constructed to remove the hydrogen-bonding phenolic hydroxyl group of the H107Y mutant, while preserving the sterical interference properties. H107N was designed with respect to the stable homologous bacterial carbonic anhydrase from *Nesseria gonorrhea* (NGCA), which has an asparagine (N99) in the analogous position to H107 in the human protein. E117 is a neighboring residue in the folded HCA II structure located in the opposite direction to H107. In NGCA this is also a glutamic acid (E109) (Figure 1b). E117 and H107 form two hydrogen bonds in the structure between the carboxyl group of E117 and the backbone and side chain of H107 (Figure 1a). An additional H-bond was implicated to be possible in the wild type structure; however, the distance is rather long (3.7 Å). The E117A mutation was generated to remove hydrogen bonds between residue 117 and 107. The double mutants H107A/E117A and H107N/E117A were made to experimentally probe the interaction energy between H107 and E117 using a double mutant cycle.

Yield and Enzyme Activity of Mutants. The proteins were expressed in *Escherichia coli* bacteria at 22 °C for 4 h, and the protein was purified by affinity chromatography. The yield of the mutants was significantly lower than the yield of pseudo wild type protein. The average yields of native protein varied for the different mutants and pseudo wild type between 1 mg/L and 70 mg/L of liquid culture (Table 1). All single mutants showed high enzyme activity (CO_2-hydration) ranging from 64 to 93% of HCA II_{pwt} (Table 1) when assayed at low temperature (incubation at 4 °C assayed in ice cold buffer 1 ± 1 °C). The double mutant H107N/E117A was almost inactive (1%), and no measurable activity was found for the H107A/E117A mutant. The relative order of enzyme activity was HCAII_{pwt} > H107A > E117A > H107F > H107N > H107Y > H107N/E117A > H107A/E117A.

Near-UV Circular Dichroism. Near-UV CD (at 4 °C) was used to obtain a fingerprint of the tertiary structure of the single mutants. The negative peaks at 270, 282, and 292 nm reflects the asymmetric structure surrounding the 7 Trp residues in HCA II (*26*). All mutants showed native like spectra but with decreased amplitudes of the peaks (Figure 2a). The decreased amplitudes reflect the increased side-chain dynamics of the mutants compared to HCA II_{pwt}, even at this low temperature. The relative order of near-UV CD signal was HCA II_{pwt} > E117A > H107N > H107A > H107F > H107Y.

Thermal Stability. The thermal stability of the protein was measured by enzyme activity and by intrinsic Trp fluorescence. HCA II_{pwt} showed a midpoint temperature of inactivation (T_{50}) at 55 °C. The data for the single mutants are summarized in Table 1, and the activity−stability curves are shown in Figure 2b. A variety of mutant stabilities were obvious from the thermal melting curves showing T_{50} values in the range of 16−40 °C for the single mutants (Figure 2b, Table 1). The least stable single mutant was the disease associated H107Y mutant. It is also apparent from a closer examination of the temperature melting curves of the mutants that there is a 10−20% pretransitional inactivation transition (Figure 2b). The double mutant (H107N/E117A) showed no activity at all, even though it was purified by affinity chromatography, which requires a native active site in the protein.

Unfolding of HCA II can be monitored by the Trp-fluorescence wavelength shift, because HCA II has seven Trp residues well distributed throughout the protein structure. In the folded protein the Trps fluoresce with a peak at 335−337 nm, in the molten globule state this peak has blue-shifted to 342−344 nm, and in the unfolded protein the Trp fluorescence peak is centered at 353−355 nm (*10*). Following the Trp wavelength maximum is a more reliable probe on global unfolding events for HCA II than changes in intensity due to energy transfer between Trp residues (*27*). By GuHCl HCA II_{pwt} unfolds via an intermediate (molten globule) in a three-state process (see below), but with thermal denaturation HCA II can only be unfolded to the molten globule state (*9*, *28*). The temperature midpoint of denaturation (T_m) for HCA II_{pwt} was 61 °C (Figure 2c, Table 1). The thermal denaturation of the mutants show that all single mutants are destabilized, showing a range of T_ms (22−40 °C) close to the T_{50} values of thermal inactivation (Table 1). The H107F mutant is

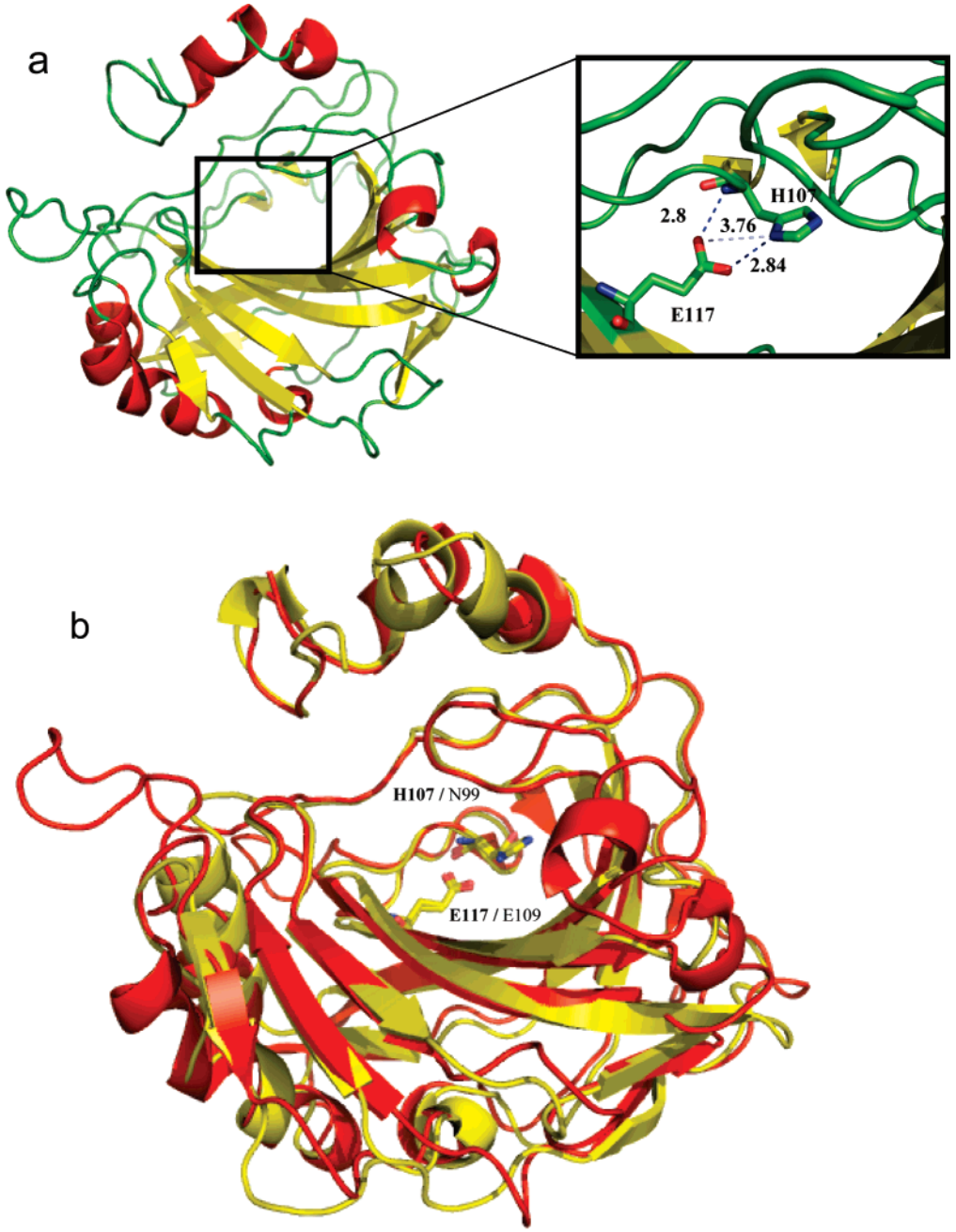

FIGURE 1: Structure of carbonic anhydrase and location of mutation sites surrounding the 107 disease mutant. (a) X-ray crystal structure of HCA II with indicated positions 107 and 117. The protein structure is dominated by a mainly antiparallel β-sheet structure spanning the entire molecule. The central cavity (framed) contains the active site. Positions 107 and 117 are closely located to the active site Zn-ion but are not directly involved in the active site. Two H-bonds and a third distant H-bond distance are indicated. The HCA II structure was obtained from pdb code 2CBA (*36*). (b) Superposition of carbonic anhydrases from human (HCA II) (red) and *Nesseria gonorrhea* (NGCA) (yellow) indicating the side chains as stick models of His107/Glu117 (HCA II) and Asn99/Glu109 (NGCA) to display the overall agreement for these residues in the three-dimensional structure. Coordinates from this figure are provided from RCSB Protein Data Bank (accession code 2CBA and 1KOP) and the figures were generated in Pymol.

almost as destabilized as H107Y, which has a T_m of 22 °C (Figure 2c and Table 1). The double mutant (H107N/E117A) shows a Trp fluorescence peak at 340 nm already at 4 °C, indicating that the protein is in the molten globule state/molten globule light state at this temperature. This also explains the minute enzyme activity of the double mutant. The double mutant H107A/E117A showed a Trp fluorescence peak at 341 nm at 4 °C (data not shown) which was even more red-shifted than that of H107N/E117A. Furthermore, the H107A/E117A mutant showed no measurable activity, indicating that this mutant was also in the molten globule state/molten globule light state at this temperature.

In summary both probes showed the following order of thermal stability:

HCA II_{pwt} > H107N > E117A > H107A > H107F > H107Y > H107N/E117A > H107A/E117A.

Temperature-Induced Aggregation. The formation of aggregates as a function of temperature was followed by right angle light-scattering measurements (330 nm). This type of aggregation measurements reflects the formation of large aggregates inducing turbidity in the sample. The aggregation

Table 1: Yield, Enzyme Activity, Thermal Stability, and Aggregation

mutant	T_m (°C)[a]	T_{50} (°C)[b]	T_a (°C)[c]	yield (mg/L)[d]	activity (% of HCA II_{pwt})[e]
HCA II_{pwt}	61	55	57	70	100
H107Y	22	16	61	6	64
H107A	32	27	55	11	93
H107F	24	21	57	9	71
H107N	40	40	59	40	65
E117A	34	33	58	32	77
H107A/E117A	≪4	ND[f]	ND	1	ND
H107N/E117A	<4	ND	ND	2	1

[a] T_m = Midpoint temperature of denaturation, monitored by Trp fluorescence. [b] T_{50} = Midpoint temperature of inactivation. [c] T_a = Midpoint temperature of aggregation. [d] Yield of pure HCA II per liter of BL21/DE3 *E. coli* culture after protein expression at 22 °C. [e] The enzyme activity was determined at 1 ± 1 °C by the CO_2 hydration assay. [f] ND = Not determined.

temperature midpoint (T_a) for HCA II_{pwt} and all mutants are all in the range 55−61 °C despite the wide variation in T_m and T_{50} values (Figure 2c, Table 1). Importantly, there was no correlation between aggregation temperature and thermal stability.

Stability toward Denaturation by GuHCl. Using GuHCl denaturation followed by the Trp-fluorescence wavelength shift enables monitoring the unfolding of HCA II to the totally unfolded state via the intermediate molten globule state. Figure 3 shows the unfolding curves for all single mutants and HCA II_{pwt}. All single mutants exhibit a three-state unfolding profile. The midpoints of denaturation for the two transitions were calculated and are summarized in Table 2. The first unfolding transition showed that the native state for all mutants is highly destabilized in comparison with HCA II_{pwt}. The unfolding of the intermediate, I → U, was independent of the introduced mutation, clearly indicating that the mutations only destabilize the tertiary structure as expected from a molten globule type intermediate. Furthermore, the Gibbs free energy of unfolding, ΔG_{NI}, was calculated from linear extrapolation as a function of GuHCl concentration. The Gibbs free energy of unfolding of the native states of the mutants was in the range 0.4−4.9 kcal/mol, to be compared with 9.6 kcal/mol for HCA II_{pwt}. The trend of stability toward chemical denaturation essentially followed that of thermal denaturation, i.e.; HCA II_{pwt} > E117A > H107N > H107A > H107F > H107Y with the exception that E117A was more stable than H107N. E117A also showed a less dynamic tertiary structure than H107N by near-UV CD at 4 °C (Figure 2a). As evident from the Trp wavelength shift the double mutants H107A/E117A and H107N/E117A are already at 0 M GuHCl in the intermediate state, and this makes it impossible to calculate midpoints of denaturation for the first transition from these data, see Table 2. This proved to be possible by the use of small molecule stabilization for H107N/E117A (see below).

Small Molecule Inhibitor Stabilization. Aromatic sulfonamide affinity chromatography purification of the double mutant H107N/E117A was successful, showing that the mutant can fold and possess a native structure in the presence of an inhibitor. However, following elution of the mutant from the sulfonamide column, the mutant partially unfolds into a molten-globule light state, which is evident from low

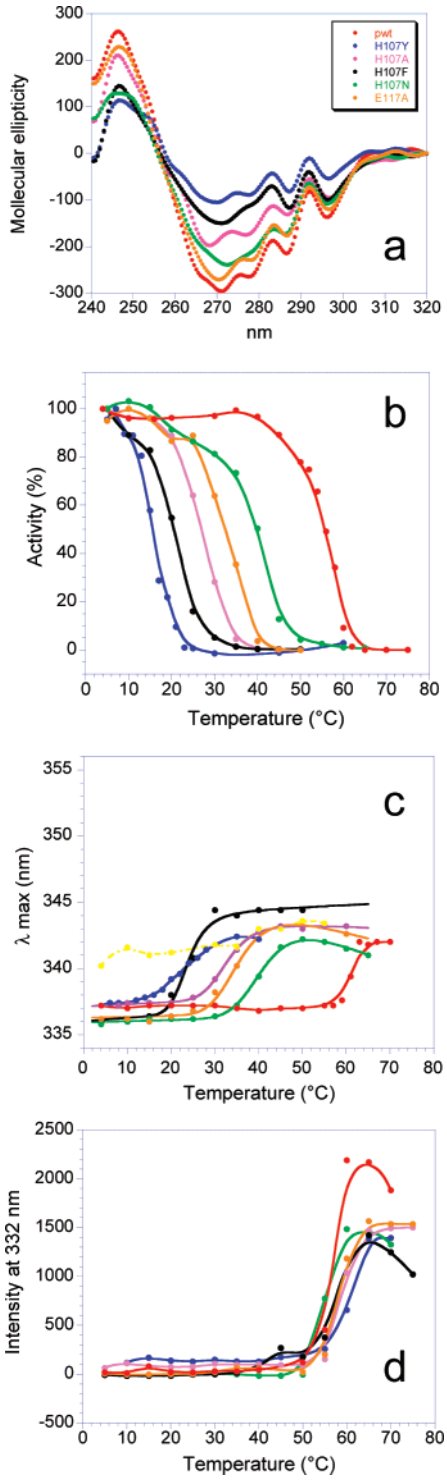

FIGURE 2: Folding and thermal stability of HCAII mutants. (a) Near UV CD spectroscopy shows the native asymmetric structure of the HCA II single mutants (symbols: H107Y (blue), H107A (pink), H107F (black), H107N (green), E117A (orange), and HCA II_{pwt} (red)). Stability toward thermal denaturation monitored by measurements of (b) enzyme activity (symbols as in a) and (c) Trp fluorescence (symbols as in a) and H107N/E117A (yellow). The protein concentration was 0.8 μM in 100 mM sodium borate, pH 7.5, in both a and b. (d) Thermal aggregation (symbols as in a). The aggregation reaction was measured by right-angle light-scattering. The protein concentration was 1.6 μM in 100 mM Tris-H_2SO_4, pH 7.5.

activity and a Trp fluorescence peak at 340 nm even at 4 °C in the absence of denaturant (see above). Since inhibitor binding was successful in affinity purification, the aromatic

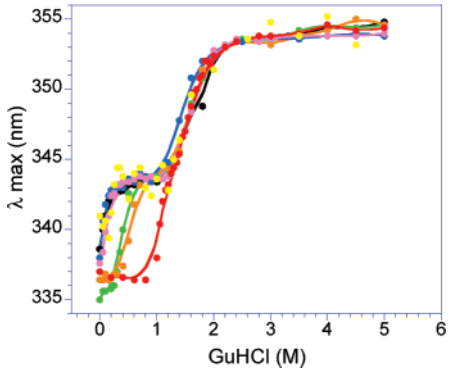

FIGURE 3: Thermodynamic stability of HCAII mutants versus GuHCl denaturation. The stability of HCA II_{pwt} (red), H107Y (blue), H107A (pink), H107F (black), H107N (green), E117A (orange), and H107N/E117A (yellow), toward denaturation by GuHCl measured by Trp fluorescence (4 °C). The protein concentration was 0.8 μM in 100 mM sodium borate buffer, pH 7.5.

sulfonamide appeared to function as a chemical chaperone to prevent misfolding by shifting the folding equilibrium toward the native state. We therefore used the small molecule inhibitor acetazolamide which has nanomolar affinity to native HCA II to induce folding of the mutant (*29*).

All mutants were incubated with acetazolamide prior to GuHCl denaturation to quantify the stability effects, $\Delta\Delta G^{Ac}$, of the inhibitor binding. The mutants were stabilized by 0.8−3.2 kcal/mol, data shown in Table 2.

Calculation of the Interaction Energy between H107 and E117. The double mutant H107N/E117A was refolded to the native state at 4 °C when preincubated with acetazolamide, and by using the data from the single mutants we could calculate the ΔG^{H_2O} value for the double mutant without inhibitor bound. In these calculations we assumed that the stabilizing effect of acetazolamide binding is an average of the effect on the two single mutants (H107N and E117A), i.e. 2.8 kcal/mol and 0.8 kcal/mol, respectively (Table 2), resulting in an average binding energy of 1.8 kcal/mol.

Hence, the calculated stability of H107N/E117A in the absence of a small molecule, ΔG_{NI} is estimated to be merely 0.1 kcal/mol; likely explaining why the H107N/E117A mutant is unfolded to the molten globule light state even at 0 M GuHCl.

From a double mutant cycle we can calculate the interaction energy (ΔG_{int}) between the H107 and E117 residues in HCA II (*30*): $\Delta G_{int} = \Delta\Delta G_{NI}^{pwt-H107N} + \Delta\Delta G_{NI}^{pwt-E117A} - \Delta\Delta G_{NI}^{pwt-H107N/E117A} = 5.4 + 4.7 - (9.6 - 0.1) = 0.6$ kcal/mol.

The total destabilization energy of the mutations in the double mutant is 9.5 kcal/mol. Hence, the interaction energy between H107 and E117 of 0.6 kcal/mol, must be regarded as almost negligible, and the destabilizing effects of the single mutations are essentially additive. This indicates independent stabilizing effects of the H107 and E117 residues. Further evidence for this comes from the double mutant H107A/E117A, which yielded a very small amount of protein during purification (Table 1) and was even less folded than H107N/E117A in buffer (see above). The theoretical stability of the H107A/E117A mutant can be estimated after subtraction of the summed destabilizations of the single mutations H107A and E117A from the stability of HCA II_{pwt}. This calculation gives a stability of −3.4 kcal/mol for H107A/E117A, showing a highly destabilized protein, which is unfolded to the molten globule light state even at low temperatures and in the absence of denaturant.

Probing Formed Molten Globules by ANS Fluorescence. The fluorescent probe ANS was used to determine the amount of intermediate formed during unfolding by GuHCl (*31*). When ANS binds to hydrophobic sites in the molten-globule state, the ANS fluorescence is blue-shifted from 520 nm for the solvent-exposed molecule to 480 nm, and the intensity is strongly augmented. The integrated intensity between 440 and 520 nm was plotted as a function of GuHCl concentration, and the amount of ANS bound to the molten-globule intermediate was determined by integrating the total ANS fluorescence in the 0−2 M GuHCl interval where all mutants and HCA II_{pwt} had a populated molten globule at GuHCl concentrations corresponding to the plateau phase of the Trp fluorescence in Figure 3. Quantification of the amount of the intermediate by the ANS fluorescence is listed in Table 2 and shows the following order of the amount of populated molten globule: H107Y > E117A > H107F > H107N, HCA II_{pwt} > H107A > H107N/E117A. Higher ANS binding to H107Y, E117A, and H107F than to HCA II_{pwt} indicates that these mutants populate both the molten globule light state and the molten globule state (*18*). The H107N mutant and HCA II_{pwt} likely only populate the molten globule state. The double mutant H107N/E117A is likely too destabilized to extensively populate both intermediates and is likely shifted toward a more unfolded state. The reason why H107A shows a decreased population of intermediate is unknown.

The data from the ANS measurements showed that the amount of the molten globule intermediate formed in the presence of acetazolamide was lower than in the absence of the inhibitor (Figure 4a; Table 2). The suppression of molten globule was especially notable at low GuHCl concentrations (<1.0 M) but was less pronounced at intermediate concentrations of GuHCl (1−2 M). This suppression effect was reported previously for H107Y (*18*) and indicates a shift in equilibrium from the molten globule states toward the native state by inhibitor binding and hence shifting the unfolding pattern of the mutants toward pseudo-wild type appearance. The suppression effect caused by a small molecule inhibitor was different for all mutants (Figure 4a). Surprisingly, there was no correlation between the amount of molten globule suppression and the extent of Gibbs free energy stabilization of acetazolamide (Figure 4b). All single mutants showed higher amounts of molten globule compared to HCA II_{pwt} in the presence of acetazolamide (Figure 4a).

Phase Diagram Analysis. Fishing for Hidden Intermediates. Analysis of protein unfolding reactions using Trp-fluorescence wavelength shifts provides a good global analysis of the protein stability. From these measurements it was evident that intermediates were populated at the plateau in the folding transition curves, as discussed above. The plateaus where molten globule and molten globule light intermediates are populated coincide with loss of enzyme activity and formation of ANS-philic carbonic anhydrase intermediates (*18*, *32*). While ANS binding has been widely used for detection of intermediates, there is also a revived way of investigating invisible population of folding intermediates which was demonstrated by the Uversky group where spectral properties reflecting quantifiable amounts of

Table 2. Protein Stability at 4 °C by GuHCl Denaturation

mutant	C_m[a] N → I (M)	C_m[a] I → U (M)	m[a] N → I	ΔG^{H_2O}[a] N → I (kcal/mol)	$\Delta\Delta G^{H_2O}$[a] (kcal/mol)	$\Delta\Delta G^{Ac}$[a] (kcal/mol)	% molten globule of pseudo-wild type[b]	% molten globule with inhibitor[b]
HCA II_{pwt}	1.05	1.62	−9.1	9.6	−		100	
H107Y	0.04	1.51	−10.5	0.4	9.2		175	
H107A	0.14	1.66	−9.3	1.3	8.3		82	
H107F	0.08	1.66	−12.8	1.0	8.6		110	
H107N	0.41	1.66	−10.4	4.2	5.4		103	
E117A	0.56	1.53	−8.7	4.9	4.7		133	
H107A/E117A	ND[c]	ND[c]	ND[c]	-3.4[e]	12.4[e]		ND	
H107N/E117A	−[c]	1.70	−[c]	−0.9[e]	10.1[e]		68	
HCA II_{pwt}+Ac[f]	−[d]	−[d]	−[d]	−[d]		−[d]		58
H107Y+Ac[f]	0.28	1.62	−12.0	3.4		3.0		68
H107A+Ac[f]	0.51	1.56	−8.8	4.5		3.2		78
H107F+Ac[f]	0.30	1.63	−7.9	2.4		1.4		98
H107N+Ac[f]	0.87	1.73	−8.1	7.0		2.8		94
E117A+Ac[f]	0.98	1.59	−5.8	5.7		0.8		66
H107N/E117A+Ac[f]	0.39	1.49	−4.8	1.9		1.8		58

[a] Measured by Trp fluorescence. [b] Measured by ANS fluorescence. [c] This mutant is in the intermediate state already at 0 M GuHCl at 4 °C. [d] Apparent single unfolding transition. [e] Calculated value, see main text for details. [f] In the presence of 10 μM acetazolamide (Ac). ND = Not determined.

different states are measured (*24*). For HCA II there is pronounced energy transfer between Trp residues which is mostly evident in the native structure and to some extent in the molten globule state (*27*). The energy transfer processes complicate the interpretation of global unfolding transitions when applying Trp fluorescence intensity measured at a single wavelength, but an analysis of combined wavelengths as a function of GuHCl could illuminate populated intermediates and their properties. To this end we selected Trp fluorescence intensities at 320 and 365 nm reflecting the amount of folded (blue-shifted) and unfolded states (red-shifted), respectively. When these parameters are plotted in an *x-y* graph, cooperative unfolding transitions should be detected as straight lines between connecting points from different concentrations of GuHCl (*24*). Figure 5a and 5b show the phase diagrams of HCA II_{pwt} and the disease mutant H107Y at 4 °C. The phase diagram for HCA II_{pwt} showed five straight well-defined transitions. Notably, the first transition (0−0.8 M GuHCl) is within the pretransitional baseline obtained with Trp fluorescence shift where the protein is folded and enzymatically active. This indicates a possible hidden intermediate, previously un-noticed. The native structure during this interval of GuHCl indicated decreased fluorescence intensity likely from side-chain dynamics inducing quenching of one or more Trps. The second transition (0.8−1.1 M GuHCl) coincides with the formation of the molten globule intermediate. The third transition occurs between 1.15 M and 1.5 M GuHCl where the molten globule starts to unfold followed by a fourth transition between 1.5 and 2.0 M GuHCl. The fifth unfolding transition occurs between 2 and 5 M GuHCl where there is an increase in the 365 nm Trp fluorescence intensity that likely reflects unfolding of residual structure (*33*) that previously has been investigated in detail by site-specific labeling of cysteine residues in the hydrophobic core (*4*, *5*, *7*, *8*).

A diverging pattern from HCA II_{pwt} was evident when the H107Y mutant was investigated in the same manner (Figure 5b). Already from 0 to 0.05 M GuHCl a dramatic difference in fluorescence intensity was observed, which correlated well with the low C_m^{N-I} of 0.04 M for H107Y by Trp fluorescence shift (Figure 3, Table 2). At GuHCl concentrations between 0.05 and 1.0 M, the H107Y mutant displayed a zigzag pattern with large amplitude differences for both fluorescence parameters. This is drastically different from the HCA II_{pwt} pattern and indicates that the H107Y mutant forms an ensemble of intermediate states in the interval 0.05−1.0 M GuHCl devoted to the molten globule light and molten globule states. In the range 1.0−3.0 M GuHCl the mutant showed one transition reflecting unfolding to the unfolded state followed by a final transition in the unfolded state (3.0−5.0 M GuHCl).

During binding to the small molecule inhibitor acetazolamide, the phase diagrams became more defined, especially for the H107Y mutant (cf. Figure 5a and 5b with Figure 5c and 5d). For H107Y in the presence of the inhibitor the diagram revealed only one broad transition from 0 to 1.2 M GuHCl where the zigzag pattern at intermediate GuHCl concentrations was suppressed correlating well with lower ANS binding in the presence of acetazolamide. For HCA II_{pwt} the molten globule transition (1.15−1.5 M GuHCl) was suppressed in the presence of the inhibitor as expected from ANS measurements.

Phase diagram plots were generated for all mutants of the study in the absence and presence of acetazolamide (Supporting Information Figure 1). In the absence of inhibitor all mutants show multiple transitions often with zigzag patterns at intermediate concentrations of GuHCl, showing that the complicated energy transfer processes within HCA II are vividly sensed in the mutants under conditions promoting population of folding intermediates. In the presence of inhibitor the profiles become well defined with a wild type like (HCA II_{pwt}) appearance.

DISCUSSION

A huge number of diseases are associated with protein misfolding. In many cases these are loss-of-function diseases where compromised protein stability renders misfolding of an important enzyme. In the gene encoding HCA II several autosomal recessive mutations have been found associated with carbonic anhydrase II deficiency syndrome also known as marble brain disease and Guibaud−Vainsel syndrome (*34*, *35*). A number of these mutations result in early translation

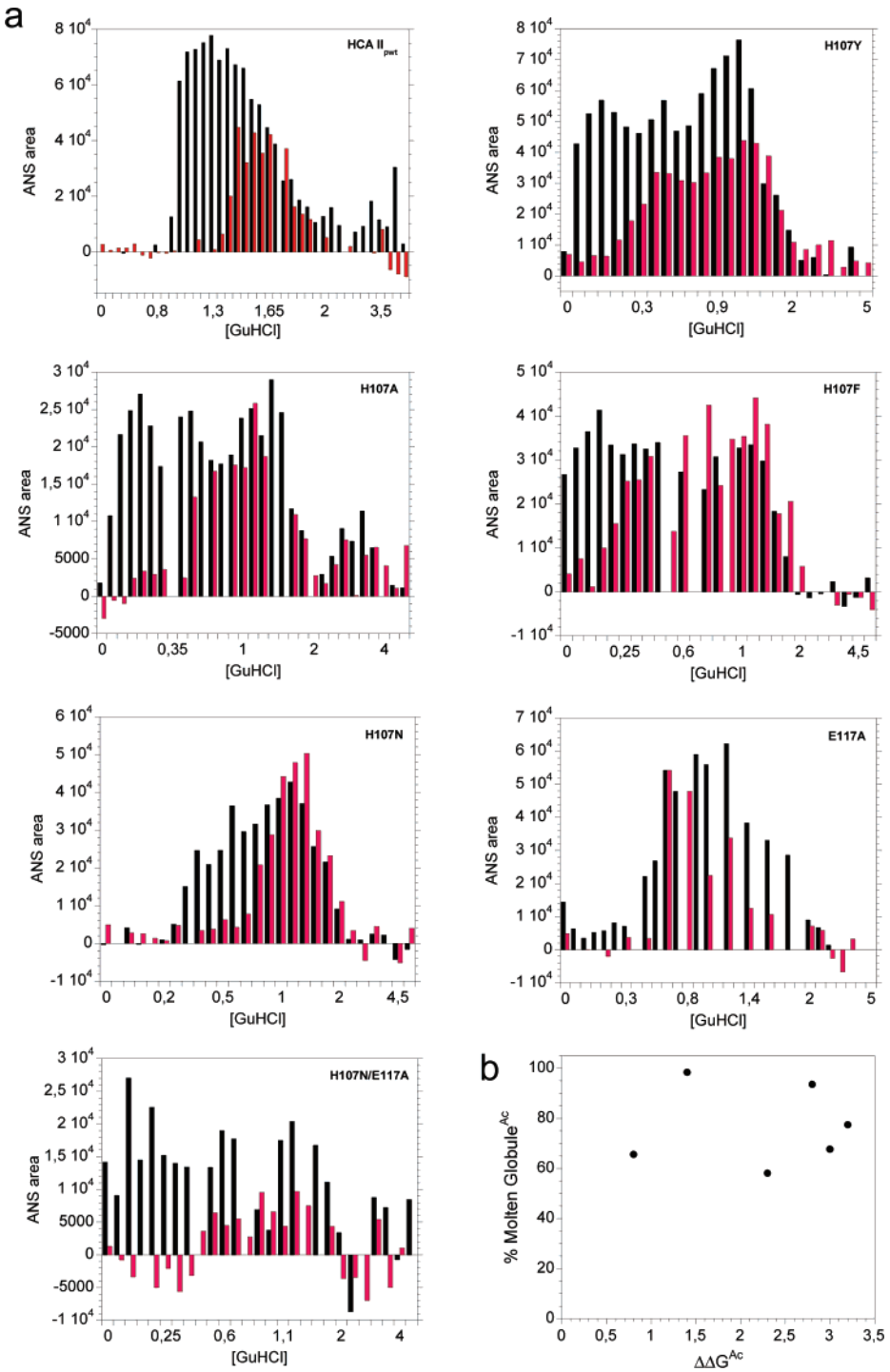

FIGURE 4: Suppression of molten globule by acetazolamide. (a) ANS fluorescence of HCA II_{pwt} and all mutants as a function of GuHCl in the presence (red bars) and absence (black bars) of the small molecule inhibitor acetazolamide. The protein concentration was 0.8 μM in 100 mM sodium borate buffer, pH 7.5, 40 μM ANS, temperature 4 °C. The final concentration of acetazolamide was 10 μM. The integrated area in the total ANS-philic interval (0−2 M GuHCl) is summarized in Table 2. (b) Lack of correlation between the suppression of molten globule, i.e., $Molten\ Globule^{Ac}$ (ANS fluorescence in the presence and absence of acetazolamide (Ac)) and the stabilizing Gibbs free energy of binding of acetazolamide ($\Delta\Delta G^{Ac}$).

termination, and others are missense point mutations (*14*−*16*). Previous data on the H107Y mutation have demonstrated that this mutant is a remarkably destabilizing folding mutation. The loss-of-function of H107Y was evidently a folding defect, since the mutant shows high CO_2-hydration activity (64%) compared to that of the wild type enzyme at low temperature, while its stability was highly compromised (*18*). In this study we confirmed that enzyme activity measured at low temperature for HCA II is a very poor probe for understanding the devastating effect of mutation in position 107. The single mutants showed high enzyme activity with no correlation to impact on protein stability and folding. Previously we have shown for other HCA II mutants that there is no correlation between stability and enzyme activity (*27*). H107 is a part of a H-bond network that originates from the active site Zn-ion ligand H119 and ends at W209 with the following sequence of residues: H119-E117-H107-Y194-S29-S197-W209 (*36*). H107 is also a

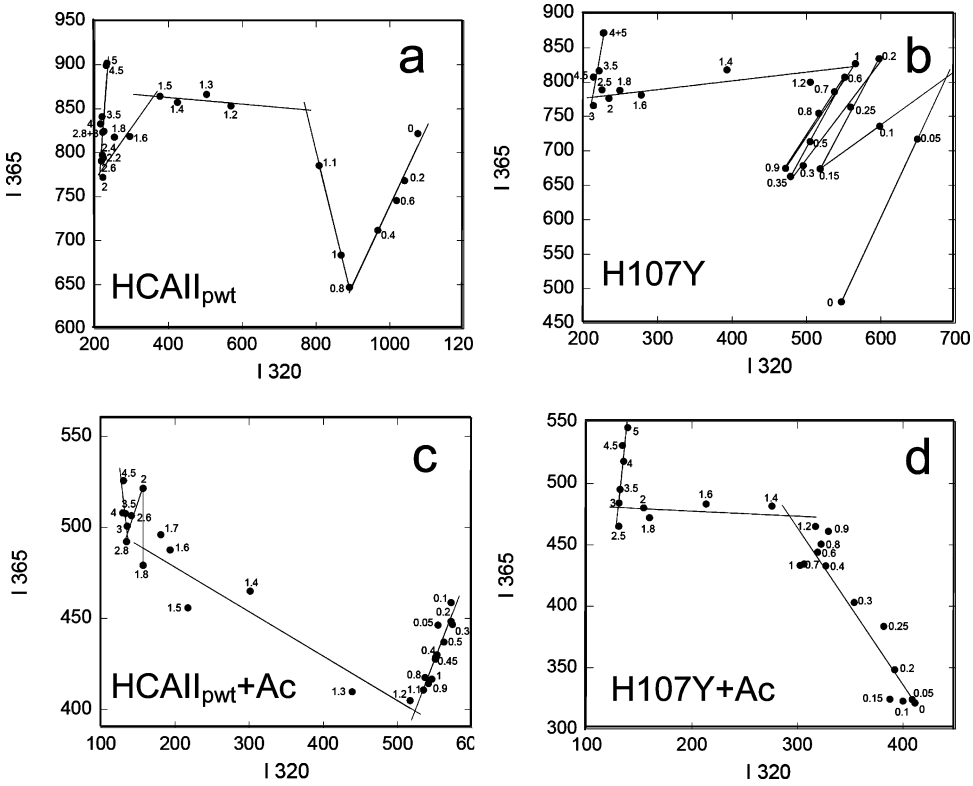

FIGURE 5: Phase diagram analysis. Tryptophan fluorescence (at 320 nm: I 320 and at 365 nm: I365) phase diagrams in various concentrations of GuHCl at 4 °C, indicated with numbers, of HCA II$_{pwt}$ and H107Y. (a and c) HCA II$_{pwt}$; (b and d) H107Y. (a and b) in the absence and (c and d) presence of 12.5 fold molar excess of the inhibitor acetazolamide (Ac); final concentration of Ac = 10 μM.

neighbor to E106 that together with T199 acts as a "doorkeeper" orienting the catalytic Zn-bound water (*37*). A possible explanation for the high activity of H107A in our study is that this mutation will induce the least sterical interference with residue 106 compared to the bulkier substitutions. The exceptional destabilization by the H107Y mutation merited to be investigated through a mutational survey to enable thermodynamic interrogation of the folding defect. Of particular interest was the finding that H107 and E117 showed two possible H-bonds in the crystal structure (Figure 1) and an implicated third H-bond. A shifted pK_a of H107 could render this residue partially charged at physiological pH (pH 7.5) to strengthen the interaction with the negatively charged H-bond partner E117. A pH variation in the erythrocyte cytoplasm (which can vary between pH 6−8) could also influence the interaction between these two residues. The E117A mutant has lower Zn-affinity (48 fold lower than wild type, but still has an association constant of 2.5×10^{10} M^{-1}) (*38*). In our studies it was evident that E117A showed the weakest binding of acetazolamide of the tested mutants which likely stems from the reported weakened Zn affinity in the active site. The interaction energy of H107 and E117 (at pH 7.5) in the wild type enzyme was calculated by comparing the energies of two single mutants and a double mutant and was found to be very low, merely 0.6 kcal/mol. Previously this method has been used to show how important salt bridges and electrostatic interactions are to the stability and folding of several proteins (*39*−*42*).

The double mutant H107A/E117A is unfolded to the molten globule light state, and H107N/E117A has an almost 0 kcal/mol ΔG of folding even at 4 °C, rendering it essentially unfolded to the molten globule light state in the absence of stabilizing small molecule inhibitor.

Notably, all mutants in position 107 are very destabilizing, demonstrating the stabilizing importance of this highly conserved histidine residue in HCA II. A reasonable linear correlation ($r = 0.945$) between the T_m and ΔG for unfolding of the native state was obtained and is shown in Figure 6a, which corroborates that temperature and GuHCl-induced unfolding likely probe the same unfolding transition, i.e., unfolding of the native state. This also holds true in the presence of the small molecule inhibitor acetazolamide. However, several outliers are evident, and interestingly these are clustered in the 30−40 °C range (Figure 6a). Importantly, all mutants populate partially folded states over a wide range of temperatures. This intermediate is not as aggregation prone as the classical molten globule state and exposes less hydrophobic surfaces and was therefore previously assigned the molten globule light state (*18*). For H107Y and H107F this preaggregation population window of the molten globule light state ranges over 40 degrees (20−60 °C) before the mutants aggregate. A cross-linking study of H107Y at 4, 25, 37, and 55 °C shows that the mutant does not form aggregates or higher order oligomers in this preaggregation temperature range at a protein concentration of 8 μM (data not shown). Hence, in contradiction to what would be expected there was no correlation between the thermal stability and the appearance of visible aggregates (Figure 6b). This shows that all the destabilized mutants in this study populate the distinct partially unfolded molten globule light state that is not as aggregation prone as the classical molten globule state which HCA II$_{pwt}$ directly populates during thermal unfolding. Furthermore we obtained no correlation between enzyme activity at low temperatures and protein stability (Table 1). We do however see significant correlation between the protein yield and protein stability (Figure 6b).

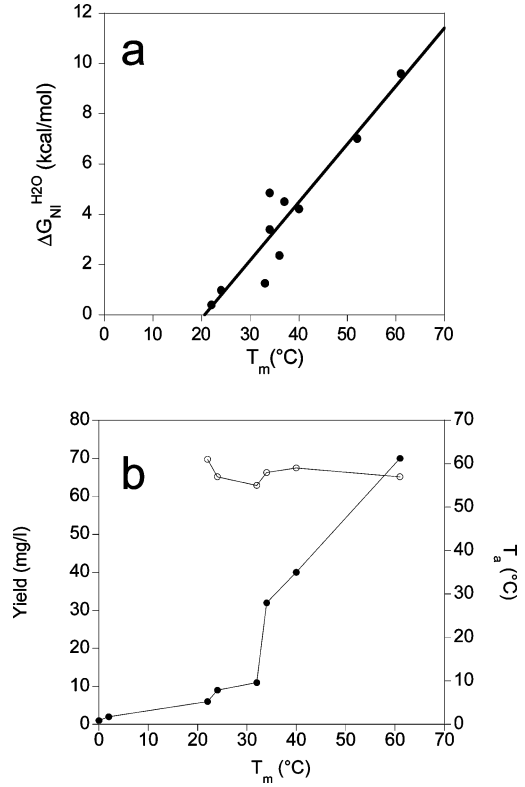

FIGURE 6: Correlation of thermal and GuHCl stability. (a) Correlation between GuHCl determined stability (4 °C) and the thermal stability (T_m) of the first unfolding transition ($\Delta G_{NI}^{H_2O}$) of HCA II_{pwt} and mutants both in the absence and presence of acetazolamide. The data fits to a linear function with a regression coefficient $r = 0.945$. (b) Correlation between yield of mutant HCA II expressed in *E. coli* at 22 °C and thermal stability (T_m), (filled circles), which indicates a transition-like curve with an increased yield for mutants with T_ms in the range 34−55 °C. The curve showing T_m versus aggregation temperature (T_a) (open circles) lacks any obvious trend showing that T_a is independent of T_m.

A very similar observation was made for mutants of p53 expressed in *E. coli* (43). Purification of HCA II from *E. coli* requires a functional active site; hence, this indicates that under *in vivo* conditions the lowered thermodynamic stability of the HCA II mutants reduce the level of folded protein. Here the protein was expressed at 22 °C and the increased yield transition cut off was at considerably higher temperatures 34−55 °C.

For GuHCl denaturation collectively the ANS and phase diagram analysis lead us to conclude the following: (i) all mutants do populate the molten globule light and molten globule states and that the molten globule light state for the mutants represents a dynamic ensemble of conformational states; (ii) the inhibitor acetazolamide functions as a chemical chaperone and suppresses the pathway leading to formation of the intermediate states and forces the mutants to behave more wild-type-like. This suppression effect is not linearly correlated to acetazolamide-induced native state stabilization. Nevertheless, the window of populating the molten globule light intermediate ensemble and the possibility to suppress this population by small molecules can be explored for structure determination of intermediates and screening for misfolding inhibitors.

In summary the thermodynamic stability of the HCA II mutants in this study was in the following order:

$HCA\ II_{pwt}$ > H107N > E117A > H107A > H107F > H107Y > H107N/E117A > H107A/E117A.

In conclusion: (i) H107N, commonly present in the analogous position in NGCA is the least destabilizing mutation likely due to compensatory H-bonding ability of the Asn side chain. (ii) Double mutant cycles surprisingly revealed additive destabilization of H107N and E117A, showing that H107 and E117 are independently stabilizing the folded protein. (iii) H107Y and H107F are exceptionally destabilizing mutations due to bulkiness of the side chains, whereas H107A is more accommodating. This indicates long-range destabilizing effects of the disease-associated H107Y mutation.

This study has shown that it can be dangerous to draw conclusions about protein stability and folding only based on interactions identified in a structural model or from enzyme activity measurements. Rather when the structural and genetic information was complemented with biophysical measurements of protein stability on a number of mutants in the position of interest and in a neighboring position, a more detailed picture of the importance of residue 107 was obtained. Nevertheless, we were surprised at the independence of the stabilizing interactions between two obvious interacting residues in the structural model. Hence, the interaction between these heavily conserved (H107 and E117) residues in carbonic anhydrases is likely not important for stability *per se* but plays essential roles as important links in the H-bond network surrounding the outer shell of the active site. To understand the consequences of mutations causing protein misfolding, one needs to take into account not only the lost native residue contacts but also possible destabilizing interactions from the introduced residue. Furthermore, compensatory interactions such as H-bonds can partially restore lost stabilizing contacts, and evidently the network of interactions in a large folded protein is rarely binary.

SUPPORTING INFORMATION AVAILABLE

Trp- fluorescence phase diagram analyses in GuHCl of HCA II mutants (at 4 °C) in the absence and presence of the inhibitor acetazolamide. This material is available free of charge via the Internet at http://pubs.acs.org.

REFERENCES

1. Boren, K., Grankvist, H., Hammarstrom, P., and Carlsson, U. (2004) Reshaping the folding energy landscape by chloride salt: impact on molten-globule formation and aggregation behavior of carbonic anhydrase, *FEBS Lett. 566*, 95−99.
2. Fransson, C., Freskgard, P. O., Herbertsson, H., Johansson, A., Jonasson, P., Martensson, L. G., Svensson, M., Jonsson, B. H., and Carlsson, U. (1992) Cis-trans isomerization is rate-determining in the reactivation of denatured human carbonic anhydrase II as evidenced by proline isomerase, *FEBS Lett. 296*, 90−94.
3. Freskgard, P. O., Bergenhem, N., Jonsson, B. H., Svensson, M., and Carlsson, U. (1992) Isomerase and chaperone activity of prolyl isomerase in the folding of carbonic anhydrase, *Science 258*, 466−468.
4. Hammarstrom, P., Owenius, R., Martensson, L. G., Carlsson, U., and Lindgren, M. (2001) High-resolution probing of local conformational changes in proteins by the use of multiple labeling: unfolding and self-assembly of human carbonic anhydrase II monitored by spin, fluorescent, and chemical reactivity probes, *Biophys. J. 80*, 2867−2885.
5. Martensson, L. G., Jonsson, B. H., Freskgard, P. O., Kihlgren, A., Svensson, M., and Carlsson, U. (1993) Characterization of folding intermediates of human carbonic anhydrase II: probing

substructure by chemical labeling of SH groups introduced by site-directed mutagenesis, *Biochemistry 32*, 224−231.
6. Persson, M., Aronsson, G., Bergenhem, N., Freskgard, P. O., Jonsson, B. H., Surin, B. P., Spangfort, M. D., and Carlsson, U. (1995) GroEL/ES-mediated refolding of human carbonic anhydrase II: role of N-terminal helices as recognition motifs for GroEL, *Biochim. Biophys. Acta 1247*, 195−200.
7. Svensson, M., Jonasson, P., Freskgard, P. O., Jonsson, B. H., Lindgren, M., Martensson, L. G., Gentile, M., Boren, K., and Carlsson, U. (1995) Mapping the folding intermediate of human carbonic anhydrase II. Probing substructure by chemical reactivity and spin and fluorescence labeling of engineered cysteine residues, *Biochemistry 34*, 8606−8620.
8. Hammarstrom, P., Kalman, B., Jonsson, B. H., and Carlsson, U. (1997) Pyrene excimer fluorescence as a proximity probe for investigation of residual structure in the unfolded state of human carbonic anhydrase II, *FEBS Lett. 420*, 63−68.
9. Hammarstrom, P., Persson, M., and Carlsson, U. (2001) Protein compactness measured by fluorescence resonance energy transfer. Human carbonic anhydrase ii is considerably expanded by the interaction of GroEL, *J. Biol. Chem. 276*, 21765−21775.
10. Hammarstrom, P., Persson, M., Freskgard, P. O., Martensson, L. G., Andersson, D., Jonsson, B. H., and Carlsson, U. (1999) Structural mapping of an aggregation nucleation site in a molten globule intermediate, *J. Biol. Chem. 274*, 32897−32903.
11. Hammarstrom, P., Persson, M., Owenius, R., Lindgren, M., and Carlsson, U. (2000) Protein substrate binding induces conformational changes in the chaperonin GroEL. A suggested mechanism for unfoldase activity, *J. Biol. Chem. 275*, 22832−22838.
12. Persson, M., Carlsson, U., and Bergenhem, N. C. (1996) GroEL reversibly binds to, and causes rapid inactivation of, human carbonic anhydrase II at high temperatures, *Biochim. Biophys. Acta 1298*, 191−198.
13. Aramaki, S., Yoshida, I., Yoshino, M., Kondo, M., Sato, Y., Noda, K., Jo, R., Okue, A., Sai, N., and Yamashita, F. (1993) Carbonic anhydrase II deficiency in three unrelated Japanese patients, *J. Inherited Metab. Dis. 16*, 982−990.
14. Hu, P. Y., Lim, E. J., Ciccolella, J., Strisciuglio, P., and Sly, W. S. (1997) Seven novel mutations in carbonic anhydrase II deficiency syndrome identified by SSCP and direct sequencing analysis, *Hum. Mutat. 9*, 383−387.
15. Shah, G. N., Bonapace, G., Hu, P. Y., Strisciuglio, P., and Sly, W. S. (2004) Carbonic anhydrase II deficiency syndrome (osteopetrosis with renal tubular acidosis and brain calcification): novel mutations in CA2 identified by direct sequencing expand the opportunity for genotype-phenotype correlation, *Hum. Mutat. 24*, 272.
16. Sly, W. S., and Hu, P. Y. (1995) Human carbonic anhydrases and carbonic anhydrase deficiencies, *Annu. Rev. Biochem. 64*, 375−401.
17. Venta, P. J., Welty, R. J., Johnson, T. M., Sly, W. S., and Tashian, R. E. (1991) Carbonic anhydrase II deficiency syndrome in a Belgian family is caused by a point mutation at an invariant histidine residue (107 His−Tyr): complete structure of the normal human CA II gene, *Am. J. Hum. Genet. 49*, 1082−1090.
18. Almstedt, K., Lundqvist, M., Carlsson, J., Karlsson, M., Persson, B., Jonsson, B. H., Carlsson, U., and Hammarstrom, P. (2004) Unfolding a folding disease: folding, misfolding and aggregation of the marble brain syndrome-associated mutant H107Y of human carbonic anhydrase II, *J. Mol. Biol. 342*, 619−633.
19. Nozaki, Y. (1972) The preparation of guanidine hydrochloride, *Methods Enzymol. 26 Pt. C*, 43−50.
20. Khalifah, R. G., Strader, D. J., Bryant, S. H., and Gibson, S. M. (1977) Carbon-13 nuclear magnetic resonance probe of active-site ionizations in human carbonic anhydrase B, *Biochemistry 16*, 2241−2247.
21. Rickli, E. E., Ghazanfar, S. A., Gibbons, B. H., and Edsall, J. T. (1964) Carbonic Anhydrases from Human Erythrocytes. Preparation and Properties of Two Enzymes, *J. Biol. Chem.239*, 1065−1078.
22. Bolen, D. W., and Santoro, M. M. (1988) Unfolding free energy changes determined by the linear extrapolation method. 2. Incorporation of delta G degrees N-U values in a thermodynamic cycle, *Biochemistry 27*, 8069−8074.
23. Myers, J. K., Pace, C. N., and Scholtz, J. M. (1995) Denaturant m values and heat capacity changes: relation to changes in accessible surface areas of protein unfolding, *Protein Sci. 4*, 2138−2148.
24. Kuznetsova, I. M., Turoverov, K. K., and Uversky, V. N. (2004) Use of the phase diagram method to analyze the protein unfolding-refolding reactions: fishing out the "invisible" intermediates, *J. Proteome Res. 3*, 485−494.
25. Chirica, L. C., Elleby, B., and Lindskog, S. (2001) Cloning, expression and some properties of alpha-carbonic anhydrase from Helicobacter pylori, *Biochim. Biophys. Acta 1544*, 55−63.
26. Freskgard, P. O., Martensson, L. G., Jonasson, P., Jonsson, B. H., and Carlsson, U. (1994) Assignment of the contribution of the tryptophan residues to the circular dichroism spectrum of human carbonic anhydrase II, *Biochemistry 33*, 14281−14288.
27. Martensson, L. G., Jonasson, P., Freskgard, P. O., Svensson, M., Carlsson, U., and Jonsson, B. H. (1995) Contribution of individual tryptophan residues to the fluorescence spectrum of native and denatured forms of human carbonic anhydrase II, *Biochemistry 34*, 1011−1021.
28. Persson, M., Hammarstrom, P., Lindgren, M., Jonsson, B. H., Svensson, M., and Carlsson, U. (1999) EPR mapping of interactions between spin-labeled variants of human carbonic anhydrase II and GroEL: evidence for increased flexibility of the hydrophobic core by the interaction, *Biochemistry 38*, 432−441.
29. Knudsen, J. F., Carlsson, U., Hammarstrom, P., Sokol, G. H., and Cantilena, L. R. (2004) The cyclooxygenase-2 inhibitor celecoxib is a potent inhibitor of human carbonic anhydrase II, *Inflammation 28*, 285−290.
30. Horovitz, A., and Fersht, A. R. (1990) Strategy for analysing the co-operativity of intramolecular interactions in peptides and proteins, *J. Mol. Biol. 214*, 613−617.
31. Semisotnov, G. V., Rodionova, N. A., Razgulyaev, O. I., Uversky, V. N., Gripas, A. F., and Gilmanshin, R. I. (1991) Study of the "molten globule" intermediate state in protein folding by a hydrophobic fluorescent probe, *Biopolymers 31*, 119−128.
32. Andersson, D., Hammarstrom, P., and Carlsson, U. (2001) Cofactor-induced refolding: refolding of molten globule carbonic anhydrase induced by Zn(II) and Co(II), *Biochemistry 40*, 2653−2661.
33. Hammarstrom, P., and Carlsson, U. (2000) Is the unfolded state the Rosetta Stone of the protein folding problem, *Biochem. Biophys. Res. Commun. 276*, 393−398.
34. Jacquemin, C., Mullaney, P., and Svedberg, E. (1998) Marble brain syndrome: osteopetrosis, renal acidosis and calcification of the brain, *Neuroradiology 40*, 662−663.
35. Muzalef, A., Alshehri, M., Al-Abidi, A., and Al-Trabolsi, H. A. (2005) Marble brain disease in two Saudi Arabian siblings, *Ann. Trop. Pediatr. 25*, 213−218.
36. Hakansson, K., Carlsson, M., Svensson, L. A., and Liljas, A. (1992) Structure of native and apo carbonic anhydrase II and structure of some of its anion-ligand complexes, *J. Mol. Biol. 227*, 1192−1204.
37. Liljas, A., Hakansson, K., Jonsson, B. H., and Xue, Y. (1994) Inhibition and catalysis of carbonic anhydrase. Recent crystallographic analyses, *Eur. J. Biochem./FEBS 219*, 1−10.
38. DiTusa, C. A., McCall, K. A., Christensen, T., Mahapatro, M., Fierke, C. A., and Toone, E. J. (2001) Thermodynamics of metal ion binding. 2. Metal ion binding by carbonic anhydrase variants, *Biochemistry 40*, 5345−5351.
39. Horovitz, A., Serrano, L., Avron, B., Bycroft, M., and Fersht, A. R. (1990) Strength and co-operativity of contributions of surface salt bridges to protein stability, *J. Mol. Biol. 216*, 1031−1044.
40. Luisi, D. L., Snow, C. D., Lin, J. J., Hendsch, Z. S., Tidor, B., and Raleigh, D. P. (2003) Surface salt bridges, double-mutant cycles, and protein stability: an experimental and computational analysis of the interaction of the Asp 23 side chain with the N-terminus of the N-terminal domain of the ribosomal protein l9, *Biochemistry 42*, 7050−7060.
41. Makhatadze, G. I., Loladze, V. V., Ermolenko, D. N., Chen, X., and Thomas, S. T. (2003) Contribution of surface salt bridges to protein stability: guidelines for protein engineering, *J. Mol. Biol. 327*, 1135−1148.
42. Tissot, A. C., Vuilleumier, S., and Fersht, A. R. (1996) Importance of two buried salt bridges in the stability and folding pathway of barnase, *Biochemistry 35*, 6786−6794.
43. Mayer, S., Rudiger, S., Ang, H. C., Joerger, A. C., and Fersht, A. R. (2007) Correlation of levels of folded recombinant p53 in escherichia coli with thermodynamic stability in vitro, *J. Mol. Biol. 372*, 268−276.

BI701720P